R. & M. No. 3766

R. & M. No. 3766

PROCUREMENT EXECUTIVE, MINISTRY OF DEFENCE

AERONAUTICAL RESEARCH COUNCIL
REPORTS AND MEMORANDA

The Effect of Damping Factor on the Behaviour of Flow Calculations in Turbomachines

PART I

The Mechanism of Damping Factor

By C. BOSMAN and M. J. HILL

PART II

Meridional Flow Calculations

By C. BOSMAN

PART III

Blade-to-Blade Flow Calculations

By C. BOSMAN, R. B. DESHPANDE and M. J. HILL

Dept. of Mechanical Engineering
University of Manchester Institute of Science and Technology

LONDON: HER MAJESTY'S STATIONERY OFFICE
1975
PRICE £1·98 NET

The Effect of Damping Factor on the Behaviour of Flow Calculations in Turbomachines

PART I by C. BOSMAN and M. J. HILL
PART II by C. BOSMAN
PART III by C. BOSMAN, R. B. DESHPANDE* and M. J. HILL

Dept. of Mechanical Engineering
University of Manchester Institute of Science and Technology

Reports and Memoranda No. 3766†
February, 1974

Summary

Part I of the report exposes the dependence of asymptotic numerical convergence upon the eigenvalues of a perturbation matrix which is a function of the principal equation of motion for the calculation of two-dimensional flows in turbomachines. The mechanism of damping factor and its limitations are thereby exposed and presented graphically. The interpretation of convergence criterion is discussed and proposals made to improve the numerical solution by extrapolation.

Part II discusses the convergence of solutions for prescribed S2 surface flows and axi-symmetric flows and shows that these are strongly influenced by the density-streamfunction relationship, leading to a Mach number limitation but being also dependent upon streamsurface twist. The principles of Part I and the theory of Part II are illustrated by numerical examples.

Part III applies and illustrates the principles of Part I to prescribed S1 streamsurfaces of revolution. It is demonstrated that a density-streamfunction relationship similar to that of Part II controls convergence behaviour of these flows but that lack of streamsurface twist conveys superior properties which are only Mach number limited.

In all cases the Mach number limitation coincides with the elliptic-hyperbolic boundary of the analytic problem.

* Now at N.G.J.E. India.
† Replaces A.R.C. 35 099.

LIST OF CONTENTS

Part I—The Mechanism of Damping Factor

1. Introduction
2. The Effect of Damping Factor
3. Convergence Behaviour
4. Extrapolating the Solution

Illustrations Figs. 1 to 6

Part II—Meridional Flow Calculations

1. Introduction
2. Analysis
3. Discussion
4. Conclusions

Table I

Illustrations Figs. 1 to 5

Part III—Blade-to-Blade Flow Calculations

1. Introduction
2. Analysis
3. Discussion
4. Conclusions

Illustrations Figs. 1 to 4

List of Symbols

References

Detachable Abstract Cards

PART I

The Mechanism of Damping Factor

by C. Bosman and M. J. Hill

1. Introduction

Finite difference solutions using fixed grids to compute the flow detail on S1 or S2 surfaces[1] in turbomachines usually derive from an equation of motion combined with the continuity equation leading to a second order partial differential equation for the streamfunction ψ. This equation together with suitable boundary conditions, when expressed in finite difference form and applied to each point of the grid, leads to a set of quasi-linear equations which may be represented after Marsh.[2]

$$M\bar{\psi} = \bar{Q}(\psi) \tag{I-1a}$$

where M is a matrix of constant coefficients, $\bar{\psi}$ is the solution vector of streamfunction values at the grid points and $\bar{Q}(\psi)$ is a non-linear vector function of the ψ's. Marsh,[2] Bosman[3] and Perkins[4] have developed schemes employing the form (I-1a) as a basis of solution for S2 surfaces while Stanitz,[5] Smith,[6] Katsanis[7] and Hill[8] have developed similar schemes for S1 surfaces of revolution. In the numerical calculation the solution is obtained by working with the form

$$\bar{\psi} = M^{-1}\bar{Q}(\psi) = \bar{c}(\psi), \tag{I-1b}$$

where the inversion of M is not carried out explicitly but some numerical equivalent is performed.

The solution to equations (I-1) is sought by an iterative scheme which adopts an arbitrary initial value $\bar{\psi}_0$ to develop a sequence of vectors $\bar{\psi}_r$ from equations (I-1), given by

$$\bar{\psi}_{r+1} = \bar{c}(\psi_r) \tag{I-2}$$

If as $r \to \infty$ $\bar{\psi}_r \to \bar{\psi}$, then the scheme converges to the solution $\bar{\psi}$ and in practice the sequence is terminated when some arbitrary convergence criterion concerning $\bar{\psi}_r$ is satisfied, the terminal vector of the sequence being accepted as a sufficient approximation to the solution. It is shown subsequently that the usual convergence criteria by themselves offer no guide to the proximity of $\bar{\psi}_r$ to the solution. The behaviour of the iterates may alternatively diverge until, if unrestrained, the temperature becomes negative leading to imaginary fluid densities or they may oscillate about a point which may or may not be the solution.

Defining a difference vector $\bar{\varepsilon}_r$ as

$$\bar{\varepsilon}_{r+1} = \bar{\psi}_{r+1} - \bar{\psi}_r \tag{I-3}$$

then by equation (I-2)

$$\bar{\varepsilon}_{r+1} = \bar{c}(\psi_r) - \bar{c}(\psi_{r-1}) \tag{I-4}$$

and since the c's are continuous analytic functions of ψ, then the Taylor expansions about the point of solution

$$\bar{c}(\psi_r) = \bar{c}(\psi) + C(\bar{\psi}_r - \bar{\psi}) + \frac{C}{2!}(\bar{\psi}_r - \bar{\psi})^2 + \ldots \tag{I-5a}$$

$$\bar{c}(\psi_{r-1}) = \bar{c}(\psi) + C(\bar{\psi}_{r-1} - \psi) + \frac{C}{2!}(\bar{\psi}_{r-1} - \bar{\psi})^2 + \ldots \tag{I-5b}$$

when differenced give by equations (I-2) and (I-3)

$$\bar{\varepsilon}_{r+1} = C\bar{\varepsilon}_r \tag{I-6}$$

neglecting second order and higher terms, where

$$C \equiv C_{ij} \equiv \frac{\partial c_i(\psi)}{\partial \psi_j}. \tag{I-7}$$

Thus equation (I-6) provides a relationship between successive difference vectors $\bar{\varepsilon}$ in the neighbourhood of the solution

$$\bar{\psi}_r - \bar{\psi} \to 0$$

and

$$\bar{\psi}_{r-1} - \bar{\psi} \to 0.$$

It is shown in the theory of matrix eigenfunctions[9,10,11] that if λ_{c_1} is distinct, then as $r \to \infty$ equation (I-6) approaches

$$\bar{\varepsilon}_{r+1} = \lambda_{c_1} \bar{\varepsilon}_r, \tag{I-8a}$$

where λ_{c_1} is the eigenvalue of C having greatest modulus i.e. dominant eigenvalue of C. The $\bar{\varepsilon}$ and λ_{c_1} may be complex, in which case they occur as the sum of a conjugate pair when equation (I-8a) leads to

$$\bar{\varepsilon}_{r+1} = 2\rho_c b_j \cos(\omega + \phi_j) \tag{I-8b}$$

where

$$\bar{\varepsilon}_r = b_j \cos \phi_j \tag{I-9}$$

and ρ_c, the spectral radius of C, is defined as

$$\rho_c \equiv |\lambda_{c_1}|. \tag{I-10}$$

It can be seen from equations (I-8) and (I-10) that the condition for convergence, $\bar{\varepsilon} \to 0$ as $r \to \infty$, is

$$\rho_c < 1. \tag{I-11}$$

2. The Effect of Damping Factor

When successive iterates $\bar{\varepsilon}_r$ show no tendency to converge or when the rate of convergence is slow, it has been found in practice that sometimes convergence can be obtained, or its rate increased, by modifying the scheme given by equation (I-2) in the following way. A further equation is introduced which allows the change in two successive vectors $\bar{\psi}_r$, $\bar{\psi}_{r+1}$ to be increased or decreased by a factor d in the following manner,

$$\bar{\psi}'_r = \bar{c}(\psi_r) \tag{I-12}$$

and

$$\bar{\psi}_{r+1} = \bar{\psi}_r + d(\bar{\psi}'_r - \bar{\psi}_r). \tag{I-13}$$

It can be seen that as $\bar{\psi}_{r+1} \to \bar{\psi}_r$ then $\bar{\psi}'_r \to \psi_r \to \psi_{r-1}$ and equation (I-2) is satisfied. Equations (I-12) and (I-13) lead to

$$\bar{\psi}_{r+1} = \bar{\psi}_r + d(\bar{c}(\psi_r) - \bar{\psi}_r) \tag{I-14}$$

when by equations (I-3), (I-4) and (I-5)

$$\bar{\varepsilon}_{r+1} = \bar{\varepsilon}_r + d(C - I)\bar{\varepsilon}_r, \tag{I-15}$$

(where I = unit matrix) which may be written

$$\bar{\varepsilon}_{r+1} = D\bar{\varepsilon}_r \tag{I-16}$$

where

$$D \equiv I + d(C - I) \tag{I-17}$$

and the condition for convergence is now (cf equation (I-11))

$$\rho_D < 1. \tag{I-18}$$

The eigenvalues are defined by the conditions[10]

$$|C - I\lambda_c| = 0 \tag{I-19}$$

and

$$|D - I\lambda_D| = 0, \tag{I-20}$$

so that substitution of expression (I-17) in condition (I-19) and rearrangement gives

$$|D - I(d\lambda_c + (1 - d))| = 0, \tag{I-21}$$

when comparison with condition (I-19) shows that the λ_D are the linear transformation

$$\lambda_D = d\lambda_c + (1 - d) \tag{I-22}$$

of the λ_c. Regarding the λ_c as vectors in the complex plane, the transformation scales them by the factor d and displaces them to the right by the $(1 - d)$. If then the λ_c all lie on and within the circular domain C of Fig. 1 then the λ_D all lie on and within the circular domain D for some $0 < d < 1$. All possible circles, tangent to the lines shown in Fig. 1, are transformations of the domain C for some value of d ($-\infty < d < \infty$), some ranges of d being indicated on the figure. For the circular domains shown (Fig. 1) the transformation may be written

$$X_D = dX_c + (1 - d) \tag{I-23}$$

and

$$R_D = dR_c. \tag{I-24}$$

The following important observations are immediate:

(i) for $d = 0$, any domain C contracts to the point $D = A$ where all $\lambda_D = 1$,
(ii) if $d < 0$ then domains C and D lie on opposite sides of the point A and
(iii) if the λ_c lie, *some to the right and some to the left of* A so that the domain C encompasses A essentially, then all transformed domains D retain this same property.

3. Convergence Behaviour

The condition (I-18) for convergence is a statement that all the λ_D must lie within the unit circle $\rho = 1$ of the complex plane (Fig. 2). It follows immediately from (ii) above that if the domain C lies to the left of A then there is some range of $d > 0$ for which convergence of expression (I-12) will occur and if the domain C lies to the right of A then there is some range of $d < 0$ for which convergence will occur. From (iii) above it follows that if the λ_c lie, some to the right and some to the left of A, then there is no value of d for which convergence is possible.

If the circular domain C (Fig. 1) is defined so that it has a minimum radius R_c which the whole spectrum λ_c lies on and within, then OE forms a convenient upper bound for ρ_c i.e.

$$OE \geqslant |\lambda_{c_1}| \equiv \rho_c. \tag{I-25}$$

In the two transformed examples of Fig. 2

$$(X_D \leqslant 0)\rho_D \leqslant OE \quad \text{and} \quad (X_D \geqslant 0)\rho_D \leqslant OF.$$

Hereforward ρ will indicate this upper bound unless the contrary is indicated.
Three special cases arise:

(i) the limiting values of d for which convergence is possible i.e. $d = d_1$ (Fig. 3a), when

$$-X_{D_1} + R_{D_1} = -1, \tag{I-26}$$

(ii) the value of d which minimises ρ_D i.e. $d = d_m$, when convergence rate is a maximum (for this case the upper bound and the true spectral radius coincide) when (Fig. 3b),

$$X_D = 0 \tag{I-27}$$

$$R_{D_m} = \rho_{D_m} = \sin \alpha, \tag{I-28}$$

(iii) the value $d = 0$ which forms the opposite limiting value for convergence, when (Fig. 3c)

$$R_D = 0 \tag{I-29}$$

$$X_D = 1. \tag{I-30}$$

It follows from the transformations (I-23), (I-24) and the above that where

$$X_D \geqslant 0 \quad \text{and} \quad d_m \geqslant d \geqslant 0, \tag{I-31}$$

$$\rho_D = 1 + 2\frac{d}{d_1}\left(1 - \frac{d_1}{d_m}\right), \tag{I-32}$$

and when

$$X_D \leqslant 0 \quad \text{and} \quad d \geqslant d_m, \tag{I-33}$$

$$\rho_D = 2\frac{d}{d_1} - 1, \tag{I-34}$$

which are plotted on Fig. 4.

Repeated application of equation (I-8a) for s iterations gives

$$\bar{\varepsilon}_{r+s} = \lambda_{D_1}^s \bar{\varepsilon}_r \tag{I-35}$$

for the transformed domain D and using the upper bound ρ_D for λ_{D_1}, the number of iterations s to obtain a given reduction ratio in the difference vectors $\bar{\varepsilon}$ is by equation (I-35)

$$s = \left(\log \frac{\varepsilon_{r+s}}{\varepsilon_r}\right) \Big/ \log \rho_D, \tag{I-36}$$

which is plotted in Fig. 5 for $\varepsilon_{r+s}/\varepsilon_r = 10^{-3}$. Since ρ_D is an upper bound for λ_{D_1} then s must be regarded as an upper bound on the number of iterations required. In Parts II and III plots of s vs d where the earlier difference vectors $\bar{\varepsilon}_r, \bar{\varepsilon}_{r+1}$ etc. are not in the neighbourhood of the solution but correspond to starting with an

arbitrary initial value $\bar{\psi}_0$, are shown for turbomachine flows on prescribed S1 and S2[1] surfaces and for axisymmetric flow. In all cases the form of Fig. 5 is apparent.

In Fig. 5 the left-hand branches derive from the locus of F (Fig. 3b) while the right-hand branch derives from the locus of E, both of which are real. If in fact the λ_D spectrum is such that ρ_D always corresponds to the complex conjugate pair λ_{D_1}, at G and H (Fig. 3b) then repeated application of equation (I-8b) gives

$$\bar{\varepsilon}_{r+s} \equiv (\varepsilon_{r+s})_j = \rho_D^s \frac{\cos(\omega s + \phi_j)}{\cos \phi_j} \tag{I-37}$$

which shows a cyclic decay with s. However a standardised measure of the convergence rate may be obtained by choosing the initial vector (equation (I-9)) such that $\cos \phi_j = \cos(\omega s + \phi_j)$ when by equation (I-37)

$$s = \left(\log \frac{\varepsilon_{r+s}}{\varepsilon_r}\right) \Big/ (\log \rho_D) \tag{I-38}$$

as for λ_{D_1} real (*see* equation (I-36)).

In this instance

$$\rho_D = \sqrt{R_D^2 + X_D^2} \tag{I-39}$$

where

$$R_D = \frac{d}{d_1}\left(2 - \frac{d_1}{dm}\right) \tag{I-40}$$

and

$$X_D = 1 - \frac{d/d_1}{d_1/dm}, \tag{I-41}$$

and the function is continuous. For a given domain of λ_c, the ρ_D corresponding to $F(X_D \geqslant 0)$ and $E(X_D \leqslant 0)$ form an upper bound, while the ρ_D corresponding to G, H form a lower bound. The bounds for s with d/d_1 are shown in Fig. 6 for $\alpha = 23{\cdot}6$ degrees.

4. Extrapolating the Solution

According to equation (I-35), the difference vectors $\bar{\varepsilon}$ are in geometric progression in the neighbourhood of the solution when λ_{D_1} is real, so that the solution $\bar{\psi}$ is available for a given $\bar{\varepsilon}_r$ if λ_{D_1} can be determined. It follows from equation (I-3) that

$$\bar{\psi} = \bar{\psi}_r + \frac{\lambda_{D_1} \bar{\varepsilon}_r}{1 - \lambda_{D_1}}. \tag{I-42}$$

Similarly when ρ_D corresponds to a complex conjugate pair $(\lambda_{D_1}, \lambda'_{D_1})$, then

$$\bar{\varepsilon}_{r+s} = \lambda_{D_1}^s(\bar{g} + i\bar{h}) + \lambda_{D_1}'^s(\bar{g} - i\bar{h}), \tag{I-43}$$

and as $s \to \infty$ the solution is given by

$$\psi_j = (\psi_r)_j + 2b_j \delta \cos(\gamma + \phi_j) \tag{I-44}$$

where ($i = \sqrt{-1}$)

$$\delta\, e^{i\gamma} = \frac{\lambda_{D_1}}{1 - \lambda_{D_1}}, \tag{I-45a}$$

$$\delta\, e^{-i\gamma} = \frac{\lambda'_{D_1}}{1 - \lambda'_{D_1}} \tag{I-45b}$$

and

$$g_j + ih_j = b_j\, e^{i\phi_j}. \tag{I-46}$$

The λ_D may be determined by any standard method[9,12] for example, from the determinants

$$(\text{real } \lambda_{D_1}) \begin{vmatrix} \bar{\varepsilon}'_r \bar{\varepsilon}_r & \bar{\varepsilon}'_r \bar{\varepsilon}_{r+1} \\ 1 & \lambda_{D_1} \end{vmatrix} = 0 \tag{I-47}$$

or

$$(\text{complex } \lambda_{D_1}) \begin{vmatrix} (\bar{\varepsilon}'_r \bar{\varepsilon}_r) & (\bar{\varepsilon}'_r \bar{\varepsilon}_{r+1}) & (\bar{\varepsilon}'_r \bar{\varepsilon}_{r+2}) \\ (\bar{\varepsilon}'_{r+1} \bar{\varepsilon}_r) & (\bar{\varepsilon}'_{r+1} \bar{\varepsilon}_{r+1}) & (\bar{\varepsilon}'_{r+1} \bar{\varepsilon}_{r+2}) \\ 1 & \lambda_{D_1} & \lambda^2_{D_1} \end{vmatrix} = 0. \tag{I-48}$$

It is also necessary to retain two successive estimates of λ_{D_1} in order to determine whether the real or complex case is appropriate and additional computer store for the three difference vectors $\bar{\varepsilon}_r, \bar{\varepsilon}_{r+1}, \bar{\varepsilon}_{r+2}$.

The convergence criterion normally used to terminate the iterates $\bar{\psi}_r$ is of the form

$$\left[\frac{(f_r)_j - (f_{r-1})_j}{(f_r)_j}\right]_{\text{for all } j} < c \tag{I-49}$$

where c is an arbitrary small value. The function f may be the streamfunction itself ψ or some function of it e.g. velocity W or density ρ.

If λ_{D_1} is real and $f = \psi$ then the criterion becomes

$$\left[\frac{(\varepsilon_r)_j}{(\psi_r)_j}\right]_{\text{for all } j} < c \tag{I-50}$$

and from equation (I-42), the departure of ψ_r from the solution is given by

$$\frac{\psi_j - (\psi_r)_j}{(\psi_r)_j} \doteq \frac{\rho_D c}{1 - \rho_D} \tag{I-51}$$

which if $\rho_D \lesssim 1$ is very large whereas if $\rho_D \gtrsim 0$ is very small. Clearly the criterion c itself is no guide to the proximity of $\bar{\psi}_r$ to the solution and the convergence rate indicated by ρ_D should also be taken into account. The above extrapolation procedure effectively circumvents this difficulty.

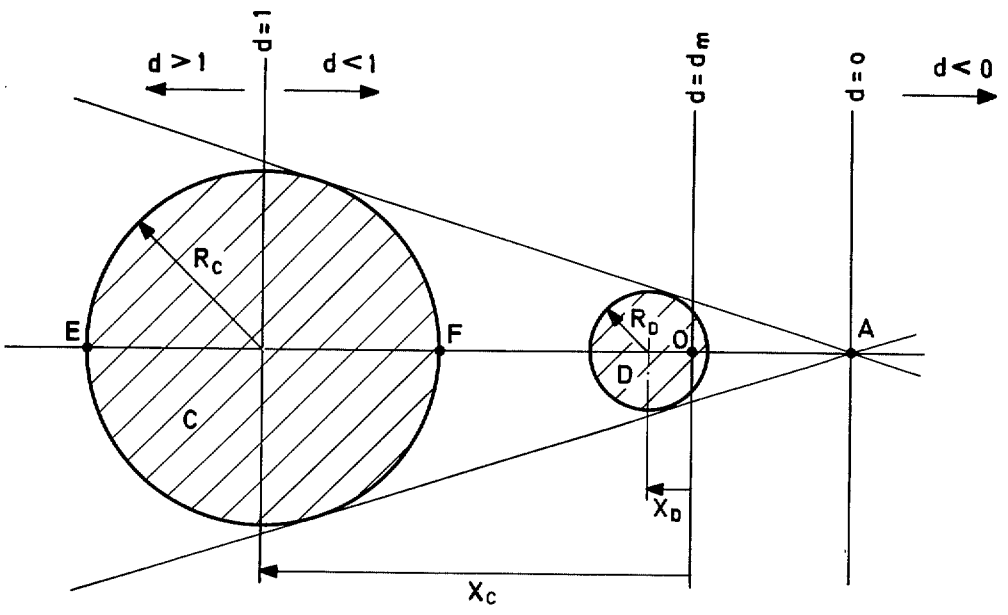

FIG. 1. The effect of damping factor d on the transformation of the domain of the λ_c to λ_D.

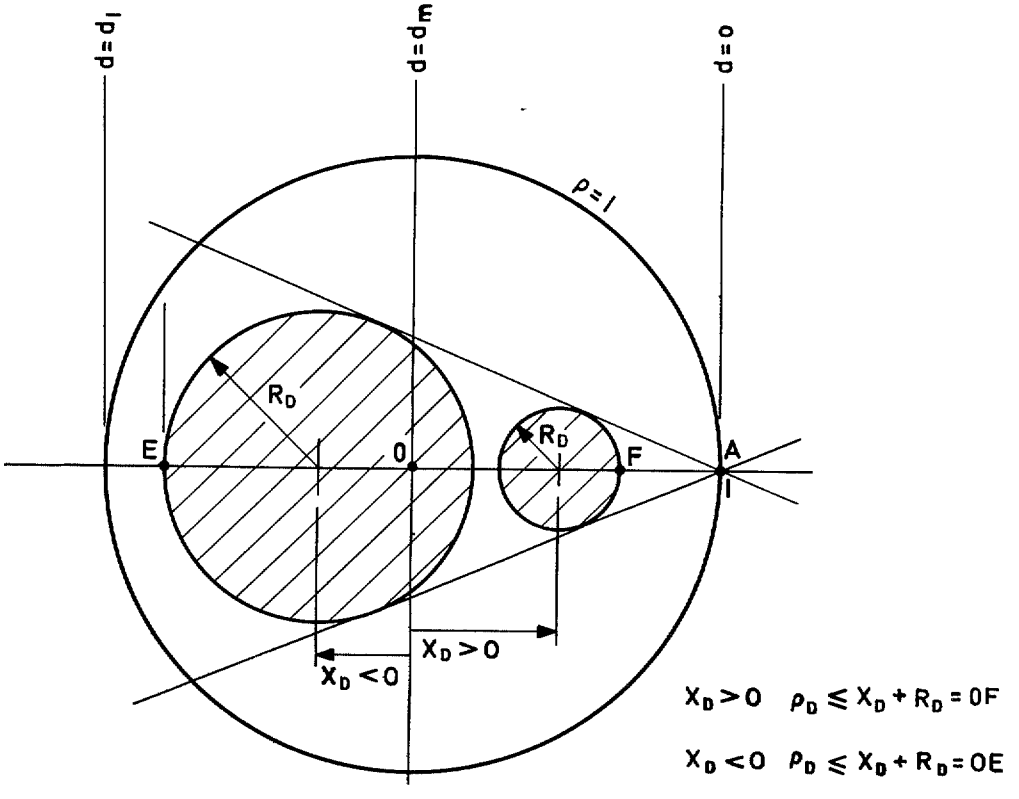

FIG. 2. Two typical domains of λ_D for which the spectral radius ρ is less than unity.

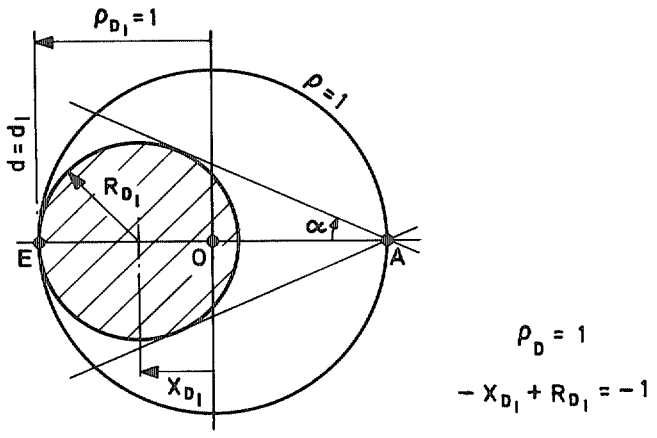

FIG. 3a. The domain of λ_D for the limiting case of convergence $d = d_1$.

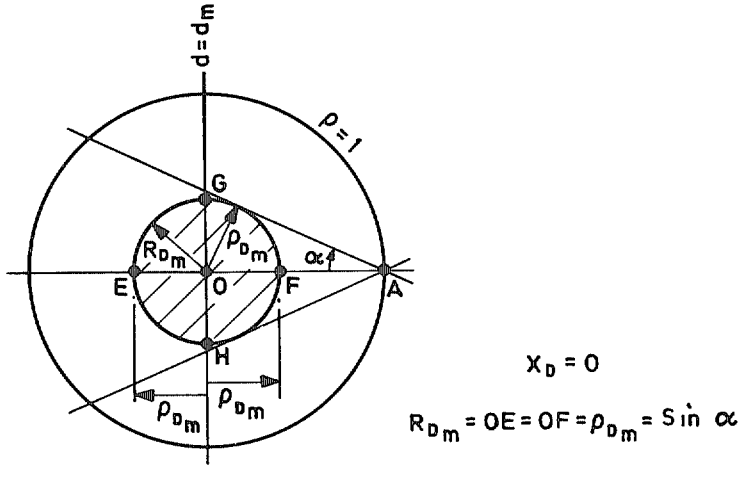

FIG. 3b. The domain of λ_D for which convergence is most rapid, when $d = d_m$.

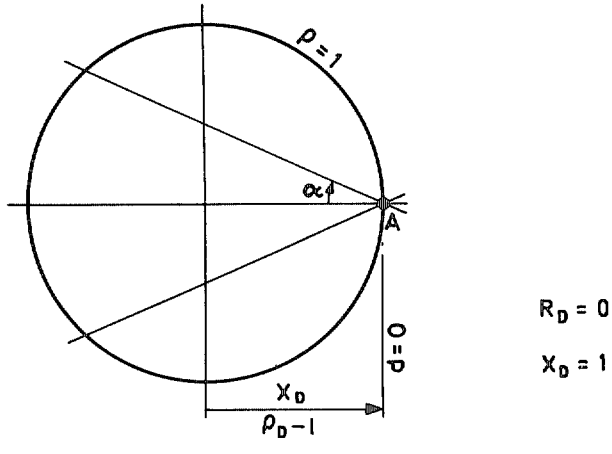

FIG. 3c. The domain of λ_D contracted to the point A for limiting convergence, when $d = 0$.

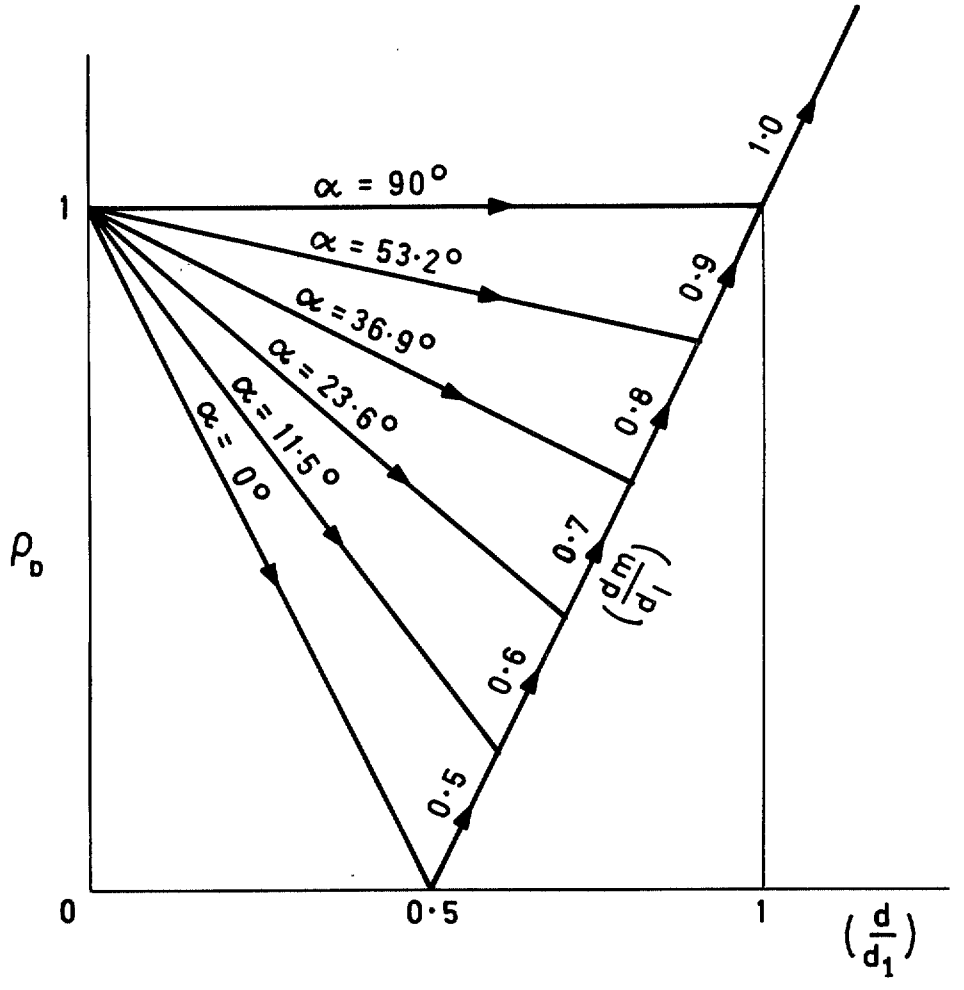

FIG. 4. The variation of the transformed spectral radius ρ_D with normalised damping factor d/d_1.

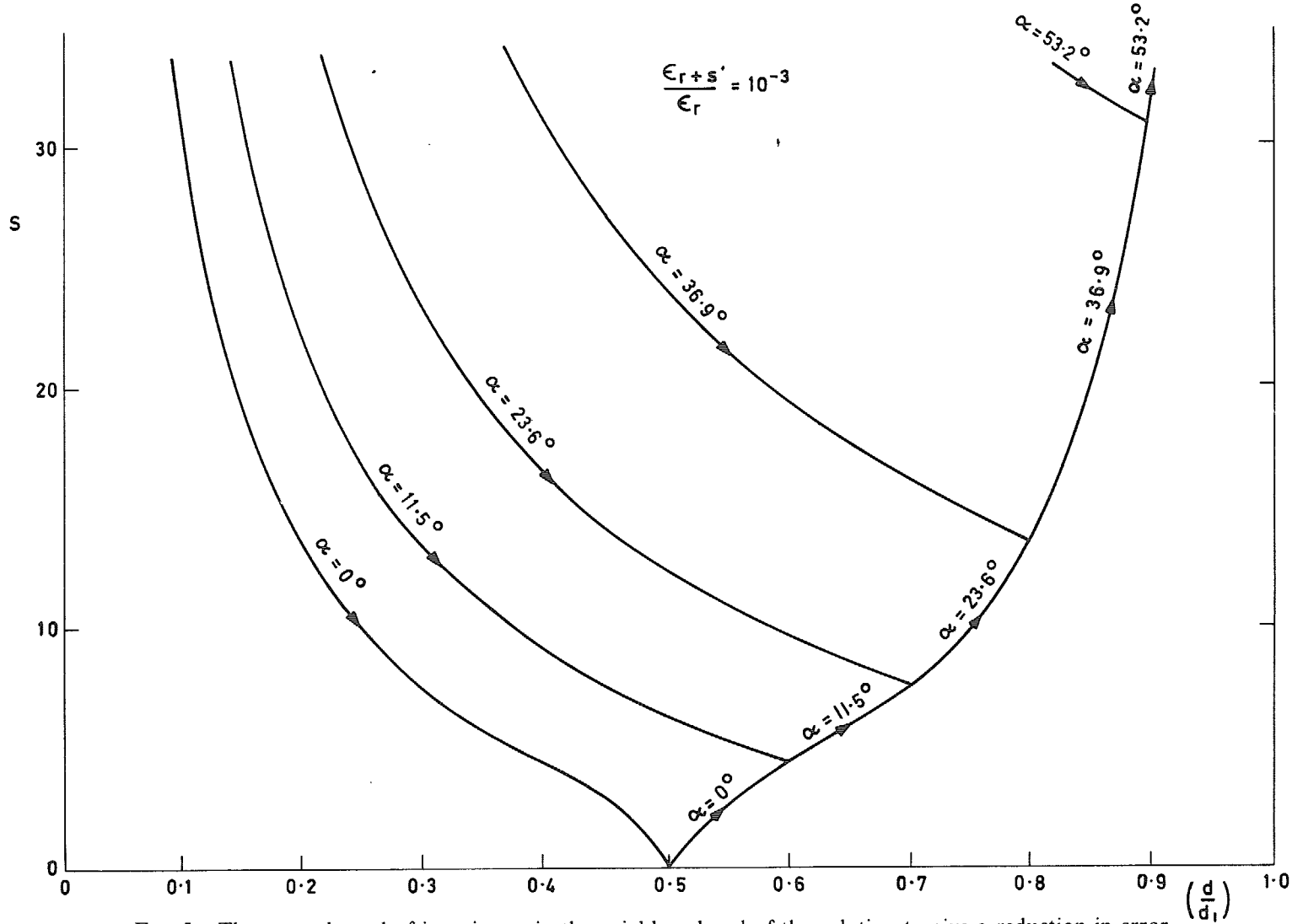

FIG. 5. The upper bound of iterations s in the neighbourhood of the solution to give a reduction in error vector ε of 10^{-3} vs normalised damping factor d/d_1 (λ_{D_1} assumed real).

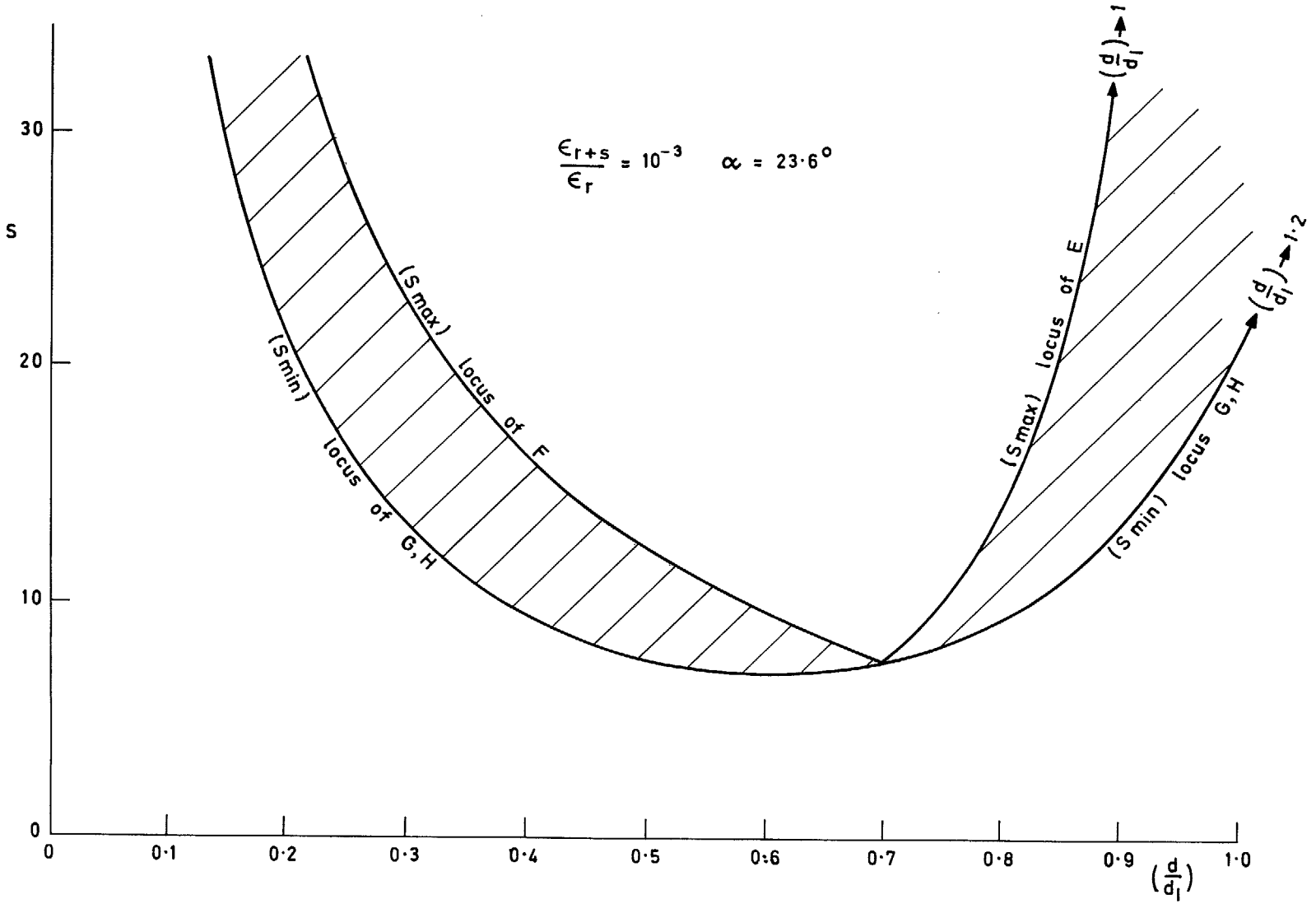

FIG. 6. The domain of upper bound iterations s in the neighbourhood of the solution to give reduction in error vector ε of 10^{-3} vs normalised damping factor d/d_1. ($\alpha = 23{\cdot}6$ and λ_{D1} may be real or complex).

PART II

Meridional Flow Calculations

by C. Bosman

1. Introduction

General experience of inviscid flow calculations for a perfect gas have shown a clear dependence of convergence behaviour upon flow Mach number. Such experience has not of itself resulted in any significant contribution to an understanding of the relationship between Mach number and convergence behaviour, while the choice a priori of a damping factor for any particular calculation is even now arbitrary and based on user experience. Johnson and Bullock[14] reported the approach to convergence failure of schemes of the type (I-1a) as Mach number approached unity while Gelder,[13] examining the irrotational, continuous problem, suggests that this type of scheme is liable to diverge if the maximum Mach number exceeds $\sqrt{1/2}$.

2. Analysis

In equation (I-1a), M represents the Laplace operator and some downstream boundary condition, being in the discrete problem a function of the flow passage and grid geometry only. Q may be written as an explicit function of ρ, ψ and grid geometry in the cases of flow for which

$$\text{grad I} = 0 = \text{grad } s \tag{II-1}$$

hence by equation (I-7)

$$C_{ij} = M^{-1}\left(\left(\frac{\partial Q_i}{\partial \rho_l}\right)_{\psi}\left(\frac{\partial \rho_l}{\partial \psi_j}\right) + \left(\frac{\partial Q_i}{\partial \psi_j}\right)_{\rho}\right). \tag{II-2}$$

Writing

$$D_r \equiv \left(\frac{\partial \psi}{\partial r}\right)_z = k_{r_i}\psi_i \tag{II-3a}$$

and

$$D_z \equiv \left(\frac{\partial \psi}{\partial z}\right)_r = k_{z_i}\psi_i \tag{II-3b}$$

where the k's are derivative coefficients in the numerical operator, then for a perfect gas, ρ is determined from

$$W_r = \frac{1}{\rho t'} D_z, \tag{II-4a}$$

$$W_z = \frac{-1}{\rho t'} D_r, \tag{II-4b}$$

$$W^2 = W_r^2 + W_\theta^2 + W_z^2, \tag{II-5}$$

$$\text{(irrotational flow) } (W_\theta + U)r = K, \tag{II-6a}$$

$$\text{(rotational axi-symmetric flow) } (W_\theta + U)r = f(\psi), \tag{II-6b}$$

$$\text{(prescribed surface flow) } W_\theta = -(W_r n_r + W_z n_z)/n_\theta, \tag{II-6c}$$

$$T = \frac{1}{Cp}\left(I - \frac{W^2 - U^2}{2}\right), \tag{II-7}$$

and

$$\frac{\rho}{\rho_1} = \left(\frac{T}{T_1}\right)^{1/k-1}. \tag{II-8}$$

Equations (II-7) and (II-8) when subject to condition (II-1) lead to

$$\frac{1}{\rho}\left(\frac{\partial \rho_l}{\partial \psi_j}\right) = \frac{-W}{kRT}\left(\frac{\partial W_l}{\partial \psi_j}\right)$$

since $U \neq$ function of ψ_j, this is written in the abbreviated form

$$\frac{d\rho}{\rho} = \frac{-W\,dW}{kRT}, \tag{II-9}$$

whereby equations (II-4) and (II-5) using similar abbreviations and remembering that $t' \neq$ function of ψ_j, lead to

(irrotational flow)

$$\frac{WdW}{kRT} = -M_m^2\frac{d\rho}{\rho} + \frac{D_r\,dD_r + D_z\,dD_z}{(kRT)(\rho t')^2}, \tag{II-10a}$$

(rotational axi-symmetric flow)

$$\frac{WdW}{kRT} = -M_m^2\frac{d\rho}{\rho} + \frac{Dr\,dD_r + D_z\,dD_z}{(kRT)(\rho t')^2} + W_\theta\frac{df}{d\psi}d\psi, \tag{II-10b}$$

(prescribed surface)

$$\frac{WdW}{kRT} = -M^2\frac{d\rho}{\rho} + \frac{1}{(kRT)(\rho t')^2}\left\{\left(1 - \frac{W_\theta n_r}{W_r n_\theta}\right)D_z\,dD_z + \left(1 - \frac{W_\theta n_z}{W_z n_\theta}\right)D_r\,dD_r\right\} \tag{II-10c}$$

where

$$M_m^2 = \frac{W_r^2 + W_z^2}{kRT} \tag{II-11}$$

is the meridional Mach number squared and

$$M^2 = \frac{W^2}{kRT} \tag{II-12}$$

is the square of the relative Mach number.

From equations (II-9) and (II-10)

(irrotational flow)

$$\frac{\partial \rho}{\partial \psi} = \frac{1}{M_m^2 - 1}\frac{1}{kRT(\rho t')^2}\left\{D_r\frac{\partial D_r}{\partial \psi} + D_z\frac{\partial D_z}{\partial \psi}\right\}, \tag{II-13a}$$

(rotational axi-symmetric flow)

$$\frac{\partial \rho}{\partial \psi} = \left\{\frac{1}{M_m^2 - 1}\frac{1}{kRT(\rho t')^2}\left(D_r\frac{\partial D_r}{\partial \psi} + D_z\frac{\partial D_z}{\partial \psi}\right) + W_\theta\frac{df}{d\psi}\right\} \tag{II-13b}$$

(prescribed surface flow)

$$\frac{\partial \rho}{\partial \psi} = \frac{1}{M^2 - 1} \frac{1}{kRT(\rho t')^2} \left\{ \left(1 - \frac{W_\theta n_r}{W_r n_\theta} \right) D_z \frac{\partial D_z}{\partial \psi} + \left(1 - \frac{W_\theta n_z}{W_z n_\theta} \right) D_r \frac{\partial D_r}{\partial \psi} \right\}. \tag{II-13c}$$

It will be observed that for plane flow where

$$W_\theta = 0, \qquad n_\theta = 1 \qquad n_r = 0 = n_z$$

and

$$M_m = M,$$

the three cases above coincide.

From equations (II-13a) and (II-13b) it can be seen that for axi-symmetric flow (rotational or irrotational) $|\partial \rho / \partial \psi| \to \infty$ as $M_m \to 1$ while for prescribed surface flows equation (II-13c), $|d\rho / \partial \psi| \to \infty$ as $M \to 1$. These conditions coincide with the boundary separating elliptic from hyperbolic flows[1] and confirm Gelder's[13] statement that the spectral radius tends to unity, usually as the problem becomes parabolic. Equation (II-13b) suggests that high swirl (W_θ) or strong gradients of absolute angular momentum ($df/d\psi$) are likely to cause increasing $|\partial \rho / \partial \psi|$ in axi-symmetric flows, while increasing amounts of streamsurface twist for which $n_\theta \to 0$ will produce similar effects in prescribed surface flows.

Unlike the term $\partial \rho / \partial \psi$, the terms $(\partial Q / \partial \rho)_\psi$ and $(\partial Q / \partial \psi)_\rho$ (*see* equation (II-2)) contain no singularities so that although they will influence C_{ij} and hence ultimate convergence rate, they do not indicate an upper stability limit for M or a lower stability limit for n_θ.

3. Discussion

Fig. 1b depicts the convergence behaviour of a calculation of the type in equation (I-1a) with various damping factors, for the inviscid flow of a perfect gas through the annular shaped nozzle of Fig. 1a, using the conformal grid there shown. Each curve shows the convergence behaviour for a streamsurface of given twist, the different streamsurfaces being prescribed in shape such that $n_r = 0$, and twisted helically according to a formula

$$\theta = \theta(z \text{ only}).$$

These streamsurfaces may be regarded as part of a flow between closely spaced guide vanes where in general the flow has swirl and since the upstream gas state and meridional velocity are the same in all cases, the Mach number increases with the rate of twist as shown in Fig. 3 where only M_{max} is plotted. The general features of Fig. 5, Part I are evident in Fig. 1b where it may be anticipated from equation (II-13c) that the coupled effect of increasing M with decreasing n_θ (i.e. higher rates of twist) will cause a rapid deterioration of convergence rate, requiring decreasing damping factors to be applied and producing a decreasing range of convergence with decreasing optimum rates. Since however each curve is for a different flow problem while the initial value is the same for all, the number of iterates to satisfy the given convergence criterion is not a certain measure of mean convergence rate and may only reflect an increasing departure of the initial value from the solution.

The common convergence criterion c (equation (I-49)) for these flows is based on velocity W with a value of 10^{-2}. Fig. 2 shows that the range of streamsurface twist for which solutions are possible using the undamped scheme is small, with a maximum throat helix angle of 40 degrees and corresponding maximum Mach number of 0·48. Reducing damping factor (Fig. 1b) makes solutions possible for increasing amounts of streamsurface twist (*see* Table I). At a twist of 0·170 (rad/axial station) the solutions obtained at the damping factors 0·4 and 0·5 differ in the region of maximum Mach number for the convergence criterion used (i.e. 10^{-2}). With increasingly fine convergence criteria M_{max} decreases towards unity as agreement is approached for different damping factors. Refining the grid also produces a reducing M_{max} and suggests that attention should be paid to both these points if accurate detail at high Mach number is required.

Damping factors in the range 0·4–0·5 would best serve these calculations from a point of view of maximum flow range with optimal convergence but this is an a posteriori observation and could not be concluded from the analysis of Part I and Section 2. The critical effect on maximum Mach number of increasing the twist can be seen from Fig. 3. as $M_{max} \to 1$, suggesting that slight disturbances of the calculation (e.g. round-off errors) will be increasingly amplified at points of high Mach number so that reducing convergence stability might be anticipated on these grounds alone. Fig. 1b suggests that the $\lambda(c)$ spectrum (*see* Part I) for these flows remains

within a region in the complex plane defined by $\alpha < 45$ degrees (Fig. 3, Part I) since (d_m/d_1) is approximately constant until $M_{max} = 1$ is closely approached but that the $\lambda(c)$ domain is moving to the left thus requiring reducing damping factors. Clearly $M_{max} = 1$ is not the limiting factor for convergence of the undamped calculation but M and n_θ are coupled in limiting the convergence at a subsonic M_{max} as equation (II-13c) would suggest. While the convergence *limit* is associated with the singularity at $M_{max} = 1$ the apparent shift of the $\lambda(c)$ spectrum to the left appears to be associated with the surface twist through decreasing n_θ and W_z (for these surfaces $n_r = 0$) and increasing values of W_θ and n_z (*see* equation (II-13c)). This is strongly indicated by the fact that when the surface is plane (i.e. $n_\theta = 1$, $n_r = 0 = n_z$) the $\lambda(c)$ remain less than unity for $M < 1$ until $M \to 1$ very closely. This is reflected in Fig. 4 which shows little change in the convergence behaviour for $d = 1$ with increasing Mach number. For plane and axi-symmetric flows generally it is a common feature that convergence can be obtained for $M_m \lesssim 1$ with $d = 1$.

In the case of fully developed, axi-symmetric, irrotational, swirling flow in a parallel annulus, individual streamsurfaces may be calculated simply, thereby permitting identical solutions to be calculated either as twisted, prescribed surface flows governed by equation (II-13c) or as axi-symmetric flows governed by equation (II-13a). Fig. 5 shows for the undamped scheme the comparative behaviour of these alternative calculations in terms of the number of iterates (s) to satisfy a given convergence criterion and the amount of prewhirl (rV_θ) imposed. Because the initial value is so close to the solution at low prewhirls the very fine convergence criterion of 10^{-6} (based on W) was necessary to show significant variation in s. The upstream gas state and meridional velocity were maintained constant throughout these examples.

Both alternative calculations show similar excellent convergence behaviour at zero prewhirl. As with the previous annular nozzle flow the surface twist limits convergence at a very low $M_{max}(= 0{\cdot}310)$ corresponding to a prewhirl of $= 60\ m^2/s$. Streamsurfaces in this flow are not unique and are generated by the paths of particles passing through any arbitrary upstream contour that crosses the stream. The values of n_θ depend upon the choice of this arbitrary upstream contour, for a particular flow case. The upstream contour in all cases was taken as a radial straight line.

When the solution is calculated as an axi-symmetric flow, Fig. 5 shows that convergence is not limited by $M_{max} = 1$ and is in fact still obtained at $M_{max} = 1{\cdot}94$. In all these cases the meridional Mach number is 0·262 which is far below the value of unity that equation (II-13a) suggests would limit convergence.

Both the analytical and numerical results here presented are at variance with the conclusions of Gelder's[13] analysis which suggests a convergence limit for $d = 1$ of $M_{max} = \sqrt{1/2}$.

4. Conclusions

Meridional, compressible flow calculations using a fixed grid and streamfunction as the variable are capable of converging to a solution using an unmodified scheme of calculation (i.e. $d = 1$) up to a limit of unit *meridional* Mach number for plane prescribed flow. Similar calculations for axi-symmetric irrotational flow continue to converge for true Mach numbers well in excess of unity when the meridional Mach number is subsonic. In both cases, theory suggests that the limit is at unity meridional Mach number and is associated with a singularity in $(\partial\rho/\partial\psi)$ at this condition which is not removed by the use of damping factor.

Flow calculations on a prescribed surface with twist may not converge to a solution when using the unmodified scheme even for very low subsonic maximum Mach numbers. The limit in these circumstances is associated with the amount of surface twist but can be extended until the maximum Mach number is unity by a suitable choice of damping factor. As in the previous case a singularity now occurs in $(\partial\rho/\partial\psi)$ which is not removed by the use of damping factor. The theory presented, whilst indicating the convergence limit due to Mach number and dependence of convergence behaviour upon surface twist, offers no guidance as to a suitable choice of value for damping factor. However, general experience suggests that the range 0·4 to 0·6 will generally lead to convergence at near optimum rate.

The Mach number limits of convergence behaviour coincide in all cases with the conditions which separate elliptic from hyperbolic flow.

TABLE I

Iterates s to satisfy convergence criterion $c(w) = 10^{-2}$ vs damping factor d for the flow given at Fig. 1a

Legend of Fig. 1a	Twist per axial station (rad)	M_{max}	Maximum helix angle (deg)
	0	0·340	0
0	0·100	0·534	49·0
Δ	0·150	0·815	59·8
∇	0·170	1·14, 1·20 (0·4), (0·5)	62·9

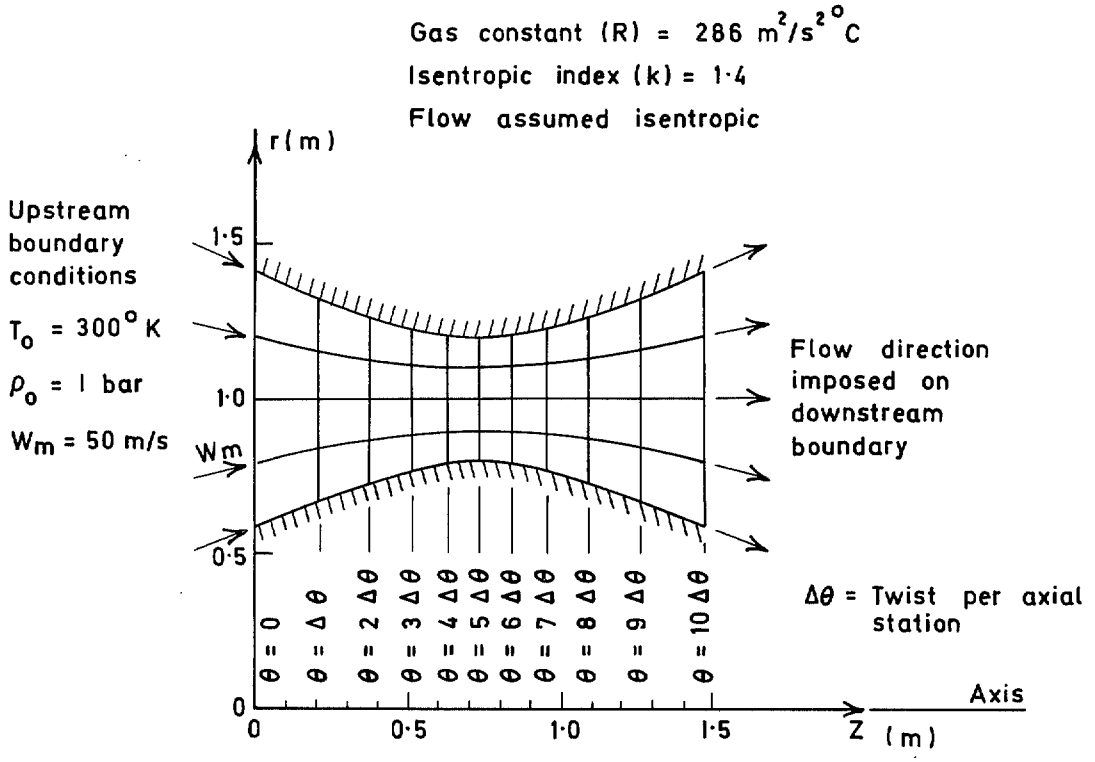

FIG. 1a. Annular nozzle. Computation grid and flow details.

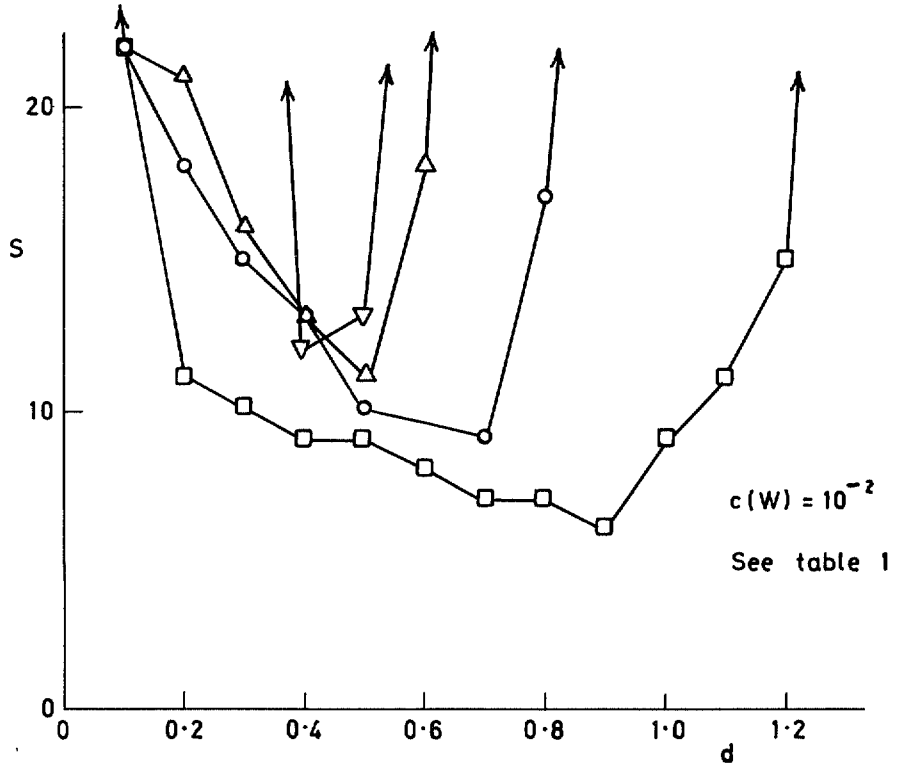

FIG. 1b. Iterates s to satisfy convergence criterion $c(w) = 10^{-2}$ vs damping factor d (see Table I for legend) for the flow given at Fig. 1a.

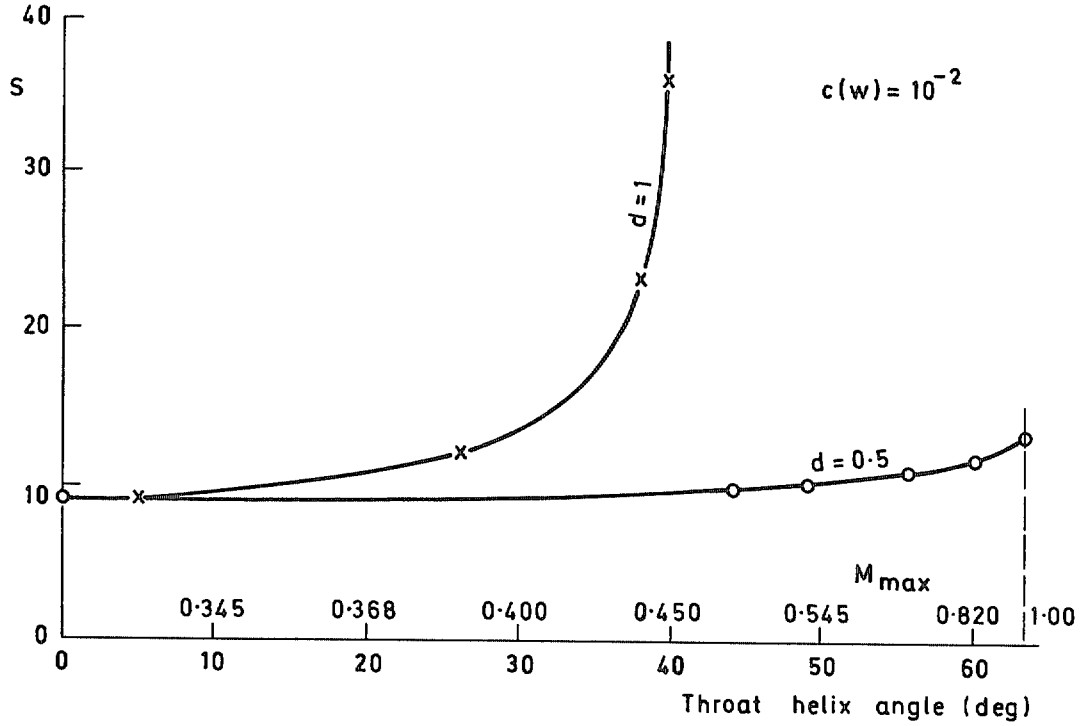

FIG. 2. Iterates s to satisfy convergence criterion $\varepsilon(w) = 10^{-2}$ vs throat helix angle for flow at Fig. 1a. Twc damping factors 1·0 and 0·5 are shown.

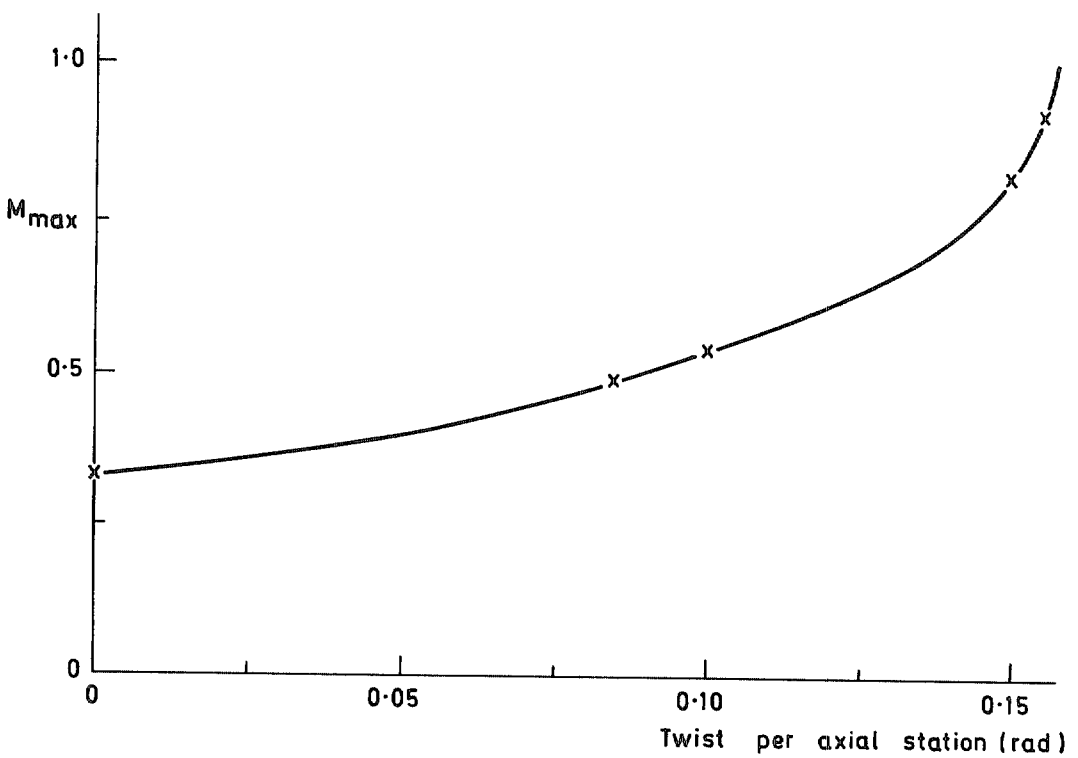

FIG. 3. Maximum flow Mach number M_{max} vs twist per axial station for the flow given at Fig. 1a.

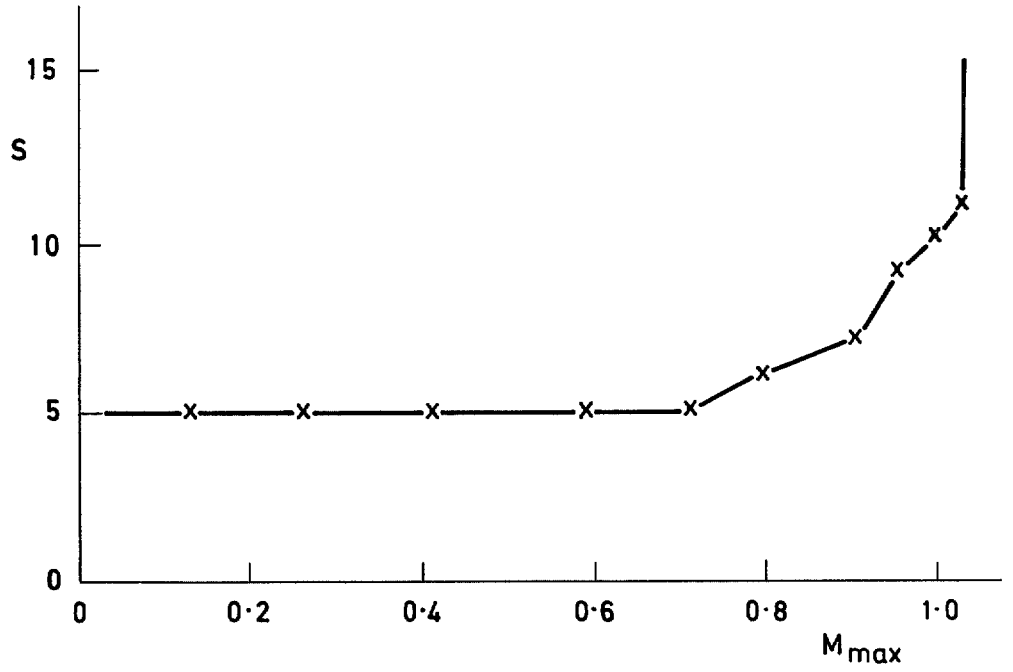

FIG. 4. Iterates s to satisfy convergence criterion $c(w) = 10^{-2}$ vs M_{max} for the flow given at Fig. 1a.

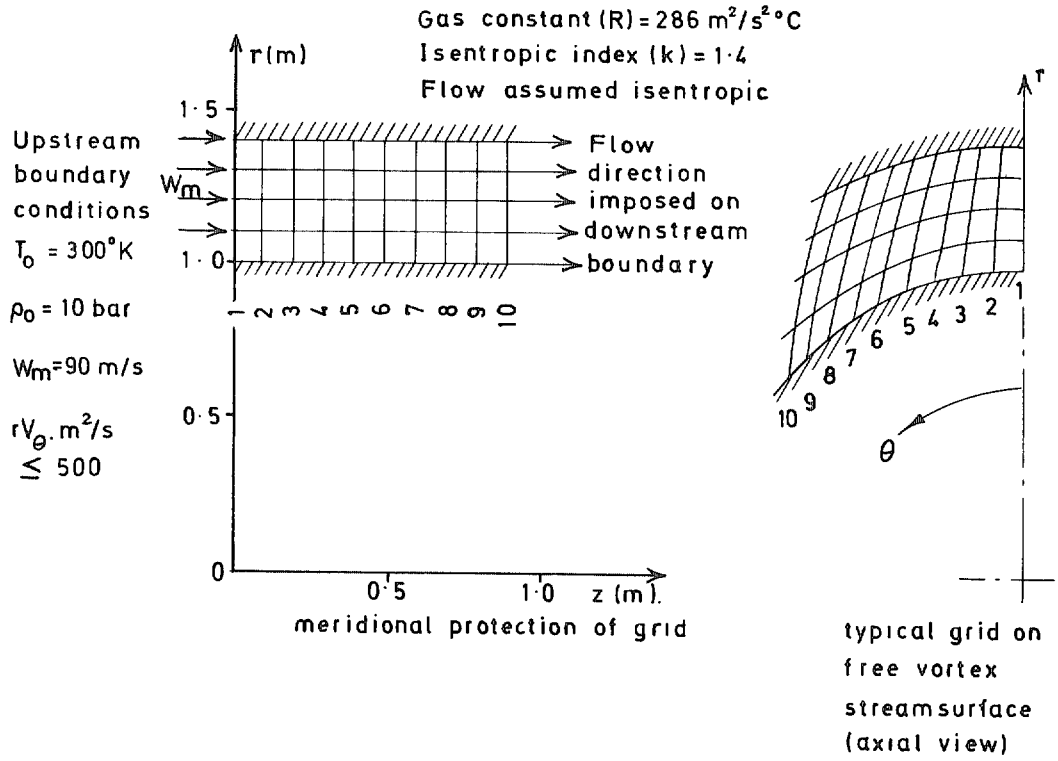

FIG. 5a. Computation grid and flow details for free vortex flow.

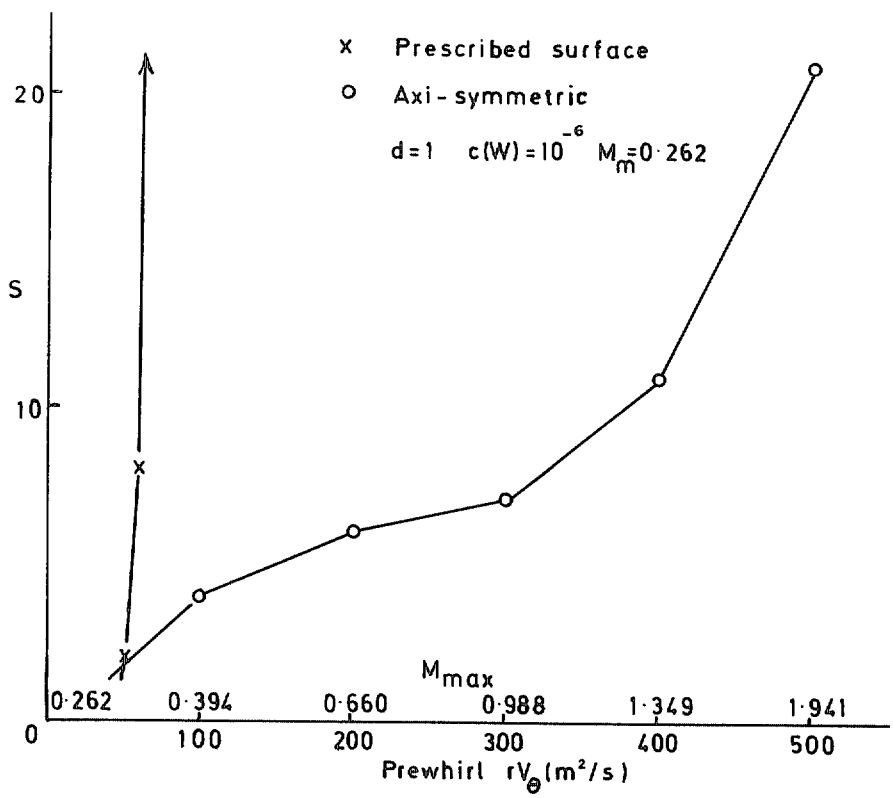

FIG. 5b. Comparison of prescribed streamsurface and axi-symmetric calculation of iterates s to satisfy convergence criterion $c(w) = 10^{-6}$ vs M_{max} and prewhirl (rV_θ). Damping factor $d = 1$.

PART III

Blade-to-Blade Flow Calculations

by C. Bosman, R. B. Deshpande and M. J. Hill

1. Introduction

In general, blade-to-blade flow calculations assume a prescribed streamsurface that is a surface of revolution and that outside the blade row the side boundary conditions are periodic. Since it is assumed that the component of vorticity normal to the streamsurface is zero, the flow is often termed irrotational and Gelder's[13] analysis applies to these cases. This type of streamsurface is curved but not twisted, as it often is in meridional flows (Part II), while the grid may be (as for meridional flows) conformal with the blade surfaces,[6] Fig. 1a, regular with blade surfaces as boundaries,[7,15] Fig. 1b, or regular with regular boundaries,[16] Fig. 1c.

2. Analysis

These flows are usually subject to the conditions

$$\text{grad } I = 0 = \text{grad } s \tag{III-1}$$

so that the analysis proceeds similarly to that in Part II for the prescribed streamsurface case but with the especially simple surface description

$$n_\theta = 0 \tag{III-2a}$$

and

$$n_r^2 + n_z^2 = 1. \tag{III-2b}$$

The velocity components are usually expressed in terms of the meridional, (m) and tangential, (θ) co-ordinate directions where

$$W_m^2 = W_r^2 + W_z^2, \tag{III-3}$$

so that from equation (I-1b)

$$C_{ij} = M^{-1}\left(\left(\frac{\partial Q_i}{\partial \rho_l}\right)_\psi \frac{\partial \rho_l}{\partial \psi_j} + \left(\frac{\partial Q_i}{\partial \psi_j}\right)_\rho\right), \tag{III-4}$$

and writing

$$D_m \equiv \left(\frac{\partial \psi}{\partial m}\right)_\theta = k_{m,i}\psi_i \qquad D_\theta \equiv \frac{1}{r}\left(\frac{\partial \psi}{\partial \theta}\right)_m = k_{\theta,i}\psi_i, \tag{III-5}$$

then

$$W_m = \frac{-1}{\rho t} D_\theta, \tag{III-6a}$$

$$W_\theta = \frac{1}{\rho t} D_m, \tag{III-6b}$$

$$T = \frac{1}{C_p}\left(I - \frac{W^2 - U^2}{2}\right) \tag{III-7}$$

and

$$\frac{\rho}{\rho_1} = \left(\frac{T}{T_1}\right)^{1/k-1}. \tag{III-8}$$

Equations (III-7) and (III-8) lead to

$$\frac{1}{\rho}\left(\frac{\partial \rho_l}{\partial \psi_j}\right) = \frac{-W}{kRT}\left(\frac{\partial W_l}{\partial \psi_j}\right)$$

since $U \neq$ function of ψ_j, this is written in the abbreviated form

$$\frac{d\rho}{\rho} = -\frac{WdW}{kRT} \tag{III-9}$$

where

$$W^2 = W_m^2 + W_\theta^2, \tag{III-10}$$

hence by equations (III-6), using similar abbreviations and remembering that $t \neq$ function if ψ_j leads to

$$\frac{WdW}{kRT} = -M^2\frac{d\rho}{\rho} + \frac{1}{(\rho t)^2 kRT}\{D_m\, dD_m + D_\theta\, dD_\theta\}, \tag{III-11}$$

when by equation (III-9),

$$\frac{\partial \rho}{\partial \psi} = \frac{1}{M^2 - 1}\cdot\frac{1}{kRT(\rho t)^2}\left\{D_m\frac{\partial D_m}{\partial \psi} + D_\theta\frac{\partial D_\theta}{\partial \psi}\right\}. \tag{III-12}$$

As the maximum relative Mach number $M_{max} \to 1$, $|\partial\rho/\partial\psi| \to \infty$ as for meridional prescribed streamsurfaces but here there is no additional complication due to streamsurface shape (*cf.* equation (II-13c)). It might be anticipated then that these flow calculations will possess superior convergence properties similar to axisymmetric and plane meridional flows (Part II) and that the upper limit of convergence will be $M_{max} = 1$.

3. Discussion

Using a computation scheme of type in equation (I-1a) and a grid as shown in Fig. 1b, the flow through the turbine stator cascade of Fig. 2a reported by Whitney *et al*[17] has been solved at zero incidence and an exit flow angle of $-67{\cdot}0$ degrees for upstream Mach numbers of 0·184 and 0·231 (corresponding maximum Mach number of 0·59 and 0·86 respectively) over a range of damping factors. The same initial value has been used in both cases with a convergence criterion of 10^{-3} based on density as used by Katsanis.[7] The number of iterates s to satisfy the convergence criterion can be seen in Fig. 2b where the form of Fig. 6 Part I is apparent and for the lower Mach number ($d_m/d_1 = 0{\cdot}6$) $\alpha = 36$ degrees while at the upper level ($d_m/d_1 > 0{\cdot}75$) $\alpha > 50$ degrees. The reducing range of d for which convergence is possible is evident from Fig. 2b, which further shows that the undamped scheme ($d = 1$) is limited to solutions with $M_{max} < 0{\cdot}59$. In order to overcome this limitation, Katsanis[7] modified this type of program[18] to fit a patch streamline curvature solution in local areas of high Mach number which then also makes transonic solutions possible, it is however possible to proceed up to $M_{max} = 1$ merely by introducing a damping factor as in equation (I-13).

Flow through this same cascade has been solved by using the same computation scheme but the alternative grid[16] of Fig. 1c. The flow conditions and convergence criterion are identical to those obtaining in Fig. 2b. The similarity of numerical behaviour using the different grids is apparent, the difference being mainly in the useful ranges of damping factor. Fortuitously it would seem, Fig. 3 shows that the grid of Fig. 1c makes solutions up to $M_{max} = 0{\cdot}86$ possible with the unmodified numerical scheme (i.e. $d = 1$) of equation (I-1) and subsequent calculations show that all flows through this blading up to $M_{max} = 1$ are possible with this grid for $d = 1$. Not only does $d = 1$ make these solutions possible but it also appears to be about an optimum value for rapid convergence. However, Fig. 2b shows that the grid of Fig. 1b offers similar optimum convergence rates to that of Fig. 1c for an appropriate choice of damping factor and further calculations show that all solutions up to $M_{max} = 1$ are possible so that neither type of grid can claim superiority.

Because each term of equation (III-4) is a complicated square matrix of values, the effect of alternative grids upon C_{ij} is not predictable in any concise terms. However the similarity of Figs. 2b and 3 with regard to d_m/d_1 and ρ_m (*see* Fig. I.4) for a given flow, indicates that

$$\rho_m = \rho_c d + (1 - d) \tag{III-13a}$$

$$= \rho_c' d' + (1 - d') \tag{III-13b}$$

where ρ_c refers to one grid and ρ_c' to the other, hence

$$\rho_c' = \rho_c\left(\frac{d}{d'}\right) + \left(1 - \frac{d}{d'}\right), \tag{III-14}$$

so that the effect of different grids upon the spectral radius of C is one of linear transformation by a single parameter (d/d') having the same form as that effected by the application of damping factor. This is to say that the two grids behave similarly with respect to convergence for a given M_{max} when plotted against (d/d_1). At low M_{max}, $d_1 = d_1'/2$.

The general form of the convergence behaviour for both the above cases is similar to that suggested by the analysis of Part I. As for meridional flows on a prescribed streamsurface (*see* Part II), increasing M_{max} increases the spectral radius ρ_D and for both types of grid the calculations fail to converge at $M_{max} = 1$ for any damping factor, as suggested by the analysis of Section 2. These observations are in keeping with those of Johnsen and Bullock[14] but contrary to the conclusions of Gelder's[13] continuous analysis which suggested a convergence limit of $M_{max} = 1/\sqrt{2}$. As Gelder comments, his analysis is not strictly valid for the schemes here employed which are not discretised by a variational method, however the weakening of his conditions implied in this application would suggest that the value of the upper convergence limit on M_{max} would probably be lowered rather than raised.

Fig. 4a shows the rotor blade shape in the $m - \theta$ plane of a radial inflow turbine with axial outlet (i.e. $V_{r_2} = 0$). The convergence behaviour of flow calculated through this rotor using a grid of the type shown in Fig. 1b can be seen in Fig. 4b. The flow has zero incidence with upstream Mach number of 0·28, approximately zero deviation and an M_{max} of 0·58. The general level of Mach number and the maximum value are similar to those of the previous axial flow turbine stator. The convergence behaviour too shows remarkable similarity (*cf.* Fig. 2b) corresponding to similar values of α. Experience has shown that generally for flows that are well subsonic, this form of grid has an upper limit of d in the region of unity with an optimum value in the region of 0·6 in contrast to grids of the type shown in Fig. 1c which generally have an optimum d in the region of unity. The former type of grid generally requires considerable reduction in d for optimum convergence at increasing M_{max}, whereas generally the latter type of grid has an optimum d which remains relatively constant for increasing M_{max}, solutions being possible for all $M_{max} < 1$ with $d = 1$.

4. Conclusions

The convergence behaviour of blade-to-blade (S1 surface) flow calculations with respect to damping factor is of the form predicted in Part I. The further analysis of Section 2 suggests an upper convergence limit of $M_{max} = 1$ where M is the Mach number relative to the blades, which is borne out by numerical experiments. The deterioration of optimum convergence rate with increasing $M_{max}(<1)$ is at best slight and the apparent reduction may only reflect on increasing departure of the initial value from the solution. Similar observations were made for meridional flows without surface twist, where the limiting condition is determined by a similar expression.

Alternative grid systems have a decisive effect on usable range of damping factor but the convergence behaviour is closely similar if plotted in terms of d/d_1. Undamped schemes and grids of the type used by Katsanis[7] have a convergence limit at low subsonic M_{max} which can be raised to unity by the introduction of damping factor. This upper limit of $M_{max} = 1$ is as observed by Johnson and Bullock[14] but at variance with the value of $\sqrt{1/2}$ suggested by Gelder.

(a)

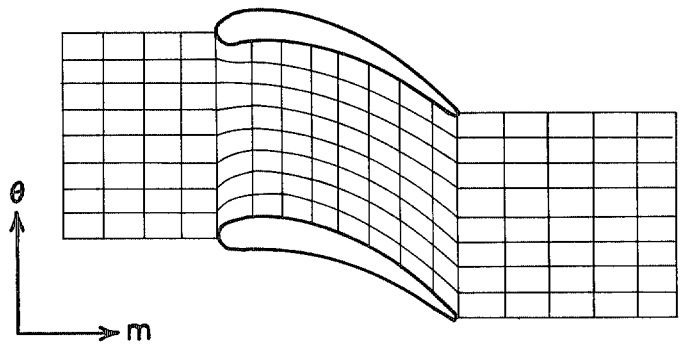

S1 surface grid as used by D. J. L. Smith.

(b)

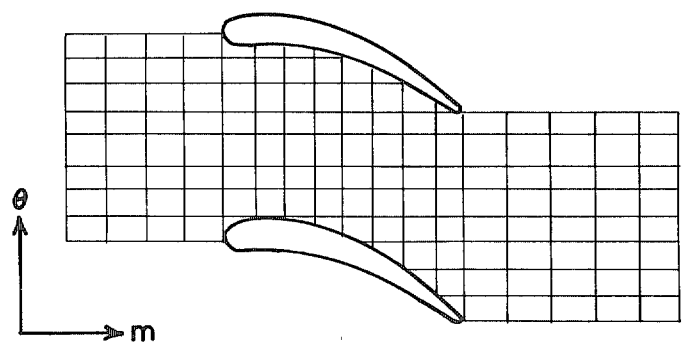

S1 surface grid as used by Katsanis, Deshpande.

(c)

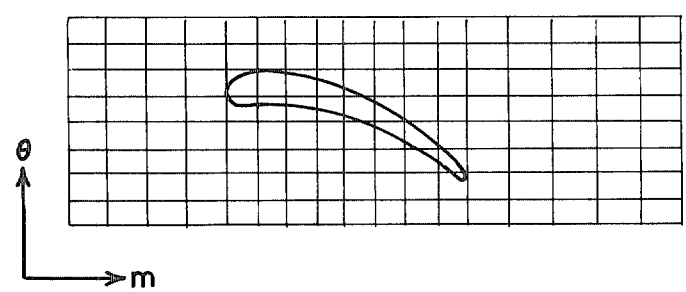

S1 surface grid as used by M. J. Hill.

FIG. 1. Various S1 surface grids used by different workers.

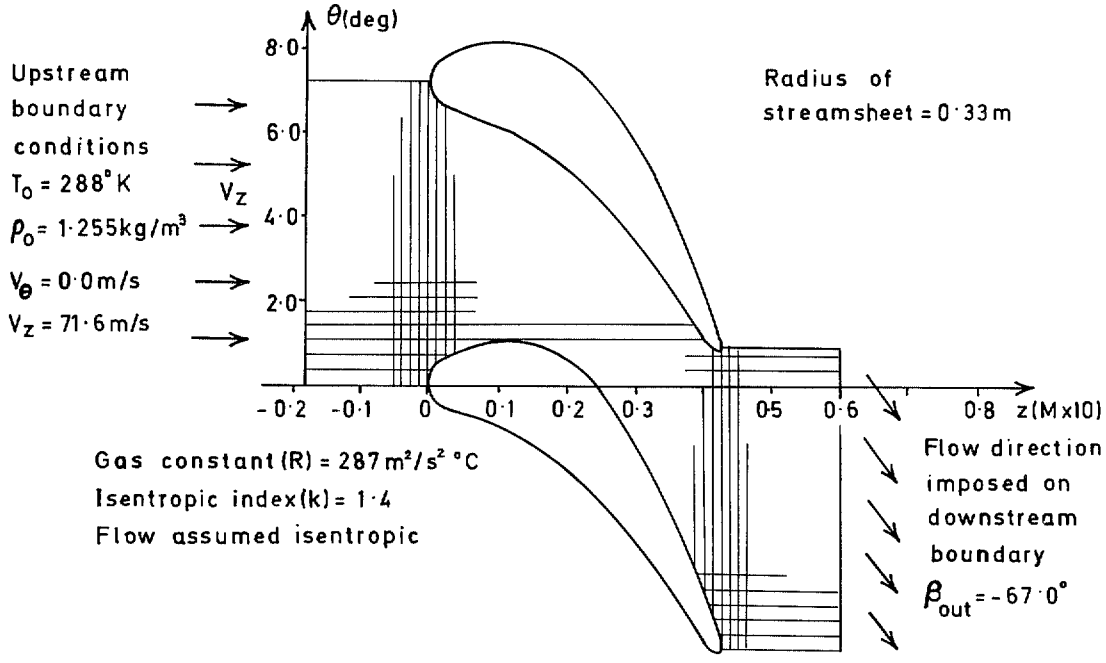

FIG. 2a. Computation grid and flow conditions for axial turbine stator.

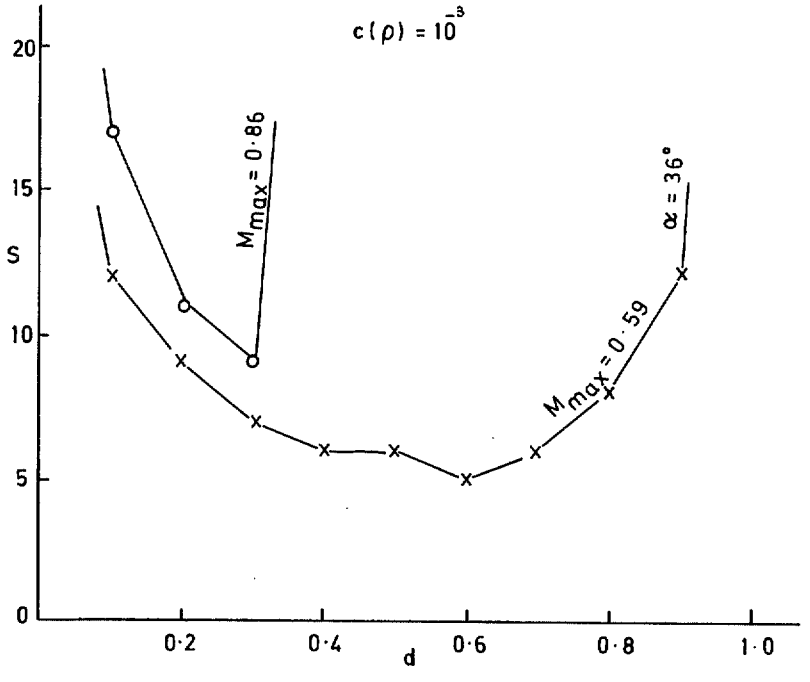

FIG. 2b. Iterates s to satisfy convergence criterion $c(\rho) = 10^{-3}$ vs damping factor d for the flow and grid given at Fig. 2a.

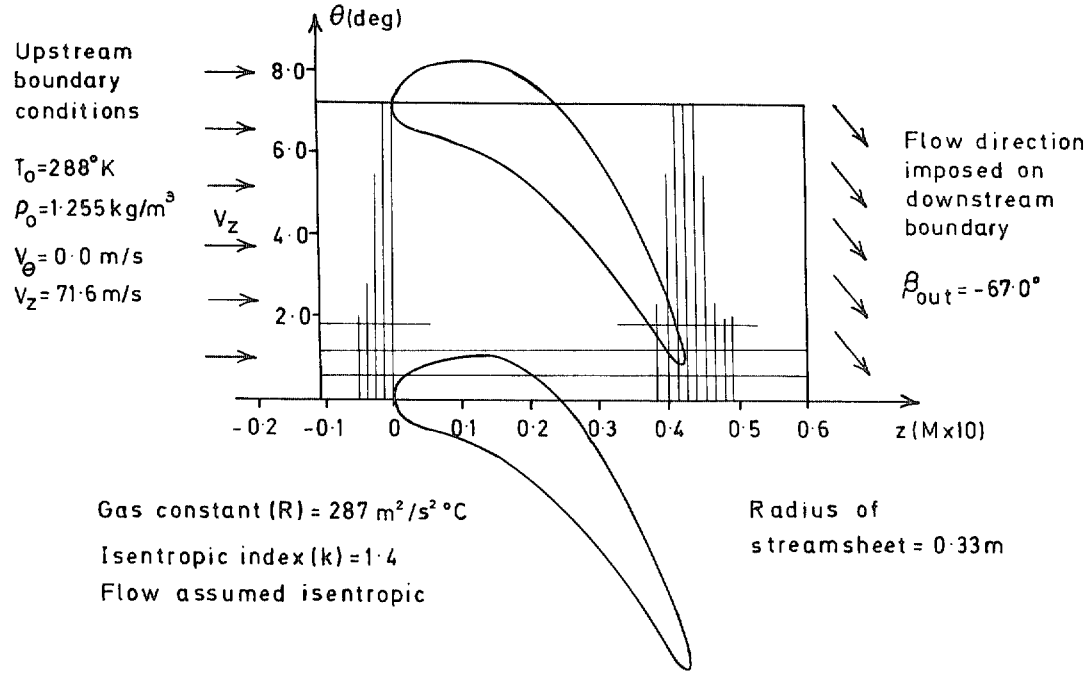

FIG. 3a. Computation grid and flow conditions for axial turbine stator.

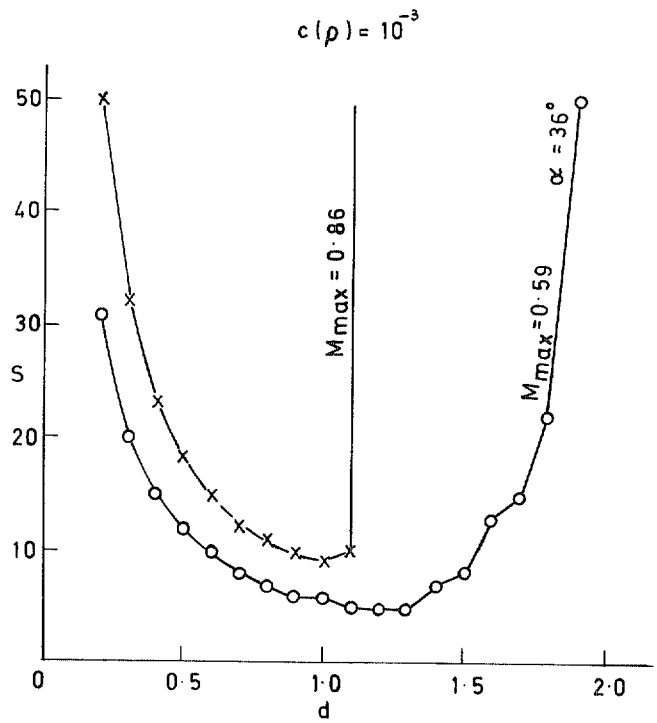

FIG. 3b. Iterates s to satisfy convergence criterion $c(\rho) = 10^{-3}$ vs damping factor d for the flow and grid given at Fig. 3a.

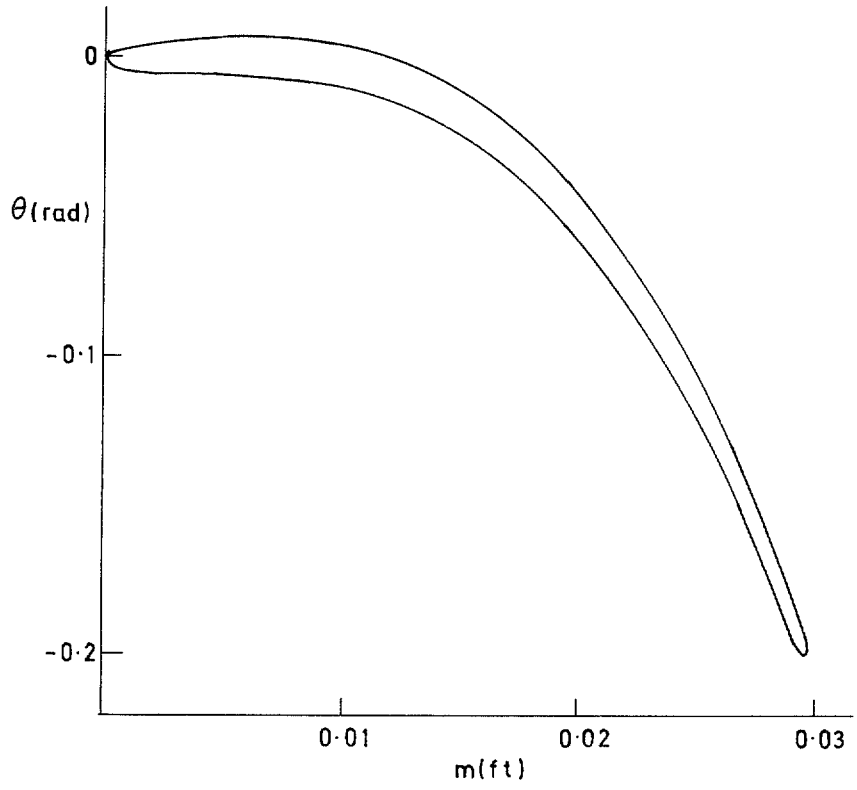

FIG. 4a. Geometrical details of radial inflow rotor blade.

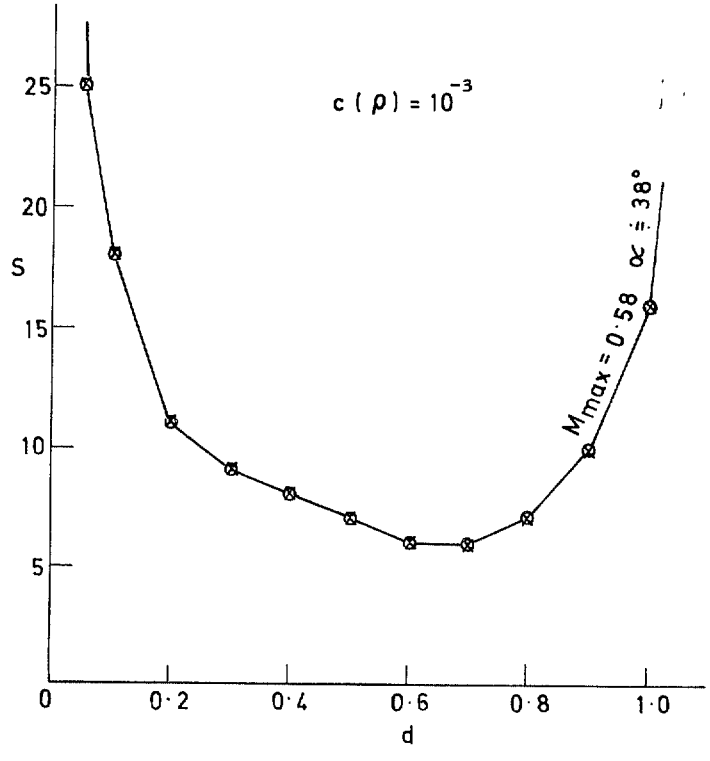

FIG. 4b. Iterates s to satisfy convergence criterion $c(\rho) = 10^{-3}$ vs damping factor d. Grid is of the type shown at Fig. 1b.

LIST OF SYMBOLS

b	Modulus of complex number (*see* eq. (I-46))
$\bar{c}$	$M^{-1}\bar{Q}$ r.h.s. of equations (*see* eq. (I-1b))
c	Convergence criterion
d, d'	Damping factors
d_1	Limiting damping factor for convergence (*see* Fig. I-3a)
d_m	Damping factor for minimum spectral radius (*see* Fig. I-3b)
e	Mathematical constant (2·718)
f	A function
g	Real part of complex number (*see* eq. (I-46))
grad	Vector operator (gradient) $= \nabla$
h	Imaginary part of complex number (*see* eq. (I-46))
i	$\sqrt{-1}$
k	Isentropic index of gas
$k_{r_i}, k_{z_i}, k_{m_i}, k_{\theta_i}$	Numerical derivative operator coefficients for directions r, z, m, θ (*see* subscripts)
n_r, n_θ, n_z	Components of streamsurface unit normal. Vector in directions, r, θ, z (*see* subscripts)
r	Radius
t	Normal thickness of streamsheet
t'	Tangential thickness of streamsheet
C, C_{ij}	Derivative matrix of vector $\bar{c}$ (*see* eq. (I-7))
C_p	Gas specific heat at constant pressure
D	Domain of transformed eigenvalues (*see* Fig. I.1)
D_r, D_z, D_m, D_θ	Space derivatives of ψ in directions r, z, m, θ (*see* eqs. (II-3) and (III-5))
I	Unit matrix
K	A constant (prewhirl)
M	L.h.s. operator matrix (*see* eq. (I-1)), relative Mach number
M_m	Meridional Mach number
$M_{\max}$	Maximum relative Mach number
Q	R.h.s. of equation (I-1a)
R	Radius of spectral domain (Pt. I. Figs. 1, 2), gas constant (Parts II, III)
T, T_1	Static temperature, temperature at arbitrary location
U	Blade speed
W	Relative speed of fluid
X	(*see* Fig. I.1)
α	Angle subtended by spectral domain (*see* Fig. I.3)
γ	Argument of complex number
δ	Modulus of complex number
$\bar{\varepsilon}_r, \bar{\varepsilon}'_r$	Difference vector of $\bar{\psi}$ at rth iterate, and its transpose (*see* eq. (I-3))

λ, λ'	Eigenvalue, and its conjugate
λ_c, λ_D	Eigenvalues in domains c and D
ρ	Spectral radius, gas density
ρ_c, ρ_D	Spectral radii of domains c and D
ϕ_j	Argument of $\bar{\varepsilon}_r$ (*see* eq. (I-9))
ψ	Streamfunction
ω	Part of argument of $\bar{\varepsilon}_{r+1}$ (*see* eq. (I-8b))

Subscripts

0	Initial value
1	Arbitrary value
c, D	Spectral domains (undamped and damped)
i, j	Tensor subscripts
r	rth iterate
r, θ, z, m	Radial, tangential, axial, meridional components
s	sth iterate

REFERENCES

No.	Author(s)	Title, etc.
1	C. H. Wu	A general theory of three-dimensional flow in subsonic or supersonic turbomachines of axial-, radial- or mixed-flow type. N.A.C.A. TN. 2604 (1952).
2	H. Marsh	A digital computer program for the through-flow fluid mechanics in an arbitrary turbomachine using a matrix method. A.R.C. R. & M. 3509 (1966).
3	C. Bosman	The occurrence and removal of indeterminacy from flow calculations in turbomachines. A.R.C. R. & M. 3746 (1973).
4	H. Perkins	Work carried out at the G.E. Co., Leicester by the turbomachine aerodynamics dept. (Classified material—not for general distribution.)
5	J. D. Stanitz and G. O. Ellis	Two-dimensional compressible flow in centrifugal compressors with straight blades. N.A.E.A. Rep. 954 (1949).
6	J. D. L. Smith and D. H. Frost	Calculations of flow past turbomachine blades. Thermo. & Fluids Conv., I.Mech.E. (1970).
7	T. Katsanis	Computer program for calculating velocities and streamlines on a blade-to-blade stream surface of a turbomachine. N.A.S.A. TND. 4525 (1968).
8	R. S. Benson, W. G. Cartwright and M. J. Hill	Analytical and experimental studies of flows in a radial bladed impeller. A.S.M.E. Paper No. 71-GT-20 Gas Turbine Conf. & Products Show, Houston, Texas (1971).
9	J. H. Wilkinson	The calculation of the latent roots and vectors of matrices on the pilot model of the A.C.E. Proc. Camb. Phil. Soc. (50) (1954).
10	W. L. Ferrar	Finite matrices. O.U.P. (1951).
11	Margenau and Murphy	The mathematics of physics and chemistry. Vol. I. Ch. 2. D. Van Nostrand Co. Inc.
12	Margenau and Murphy	The mathematics of physics and chemistry. Vol. 2. Ch. 6. D. Van Nostrand Co. Inc. (1964).
13	D. Gelder	Solution of the compressible flow equations. Int. Jour. of Num. Methods in Eng. Vol. 3 (1971).
14	I. A. Johnson and R. O. Bullock	Aerodynamic design of axial flow compressors. Ch. V. N.A.S.A. SP-36 (1965).
15	R. B. Deshpande	A comparison and optimisation of computation techniques for inviscid blade-to-blade flow through a turbomachine. Ph.D. Thesis, U.M.I.S.T., Manchester (1971).

16 M. J. Hill .. .. Numerical solutions for mixed flow turbomachines.
Ph.D. Thesis, U.M.I.S.T., Manchester (1974).

17 W. J. Whitney, E. M. Szanca, T. P. Moffitt and D. E. Monroe
Cold-air investigation of a turbine for high temperature engine application.
I. Turbine design and overall stator performance.
N.A.S.A. TND. 3751 (1967).

18 T. Katsanis .. .. Fortran program for calculating transonic velocities on a blade-to-blade surface of a turbomachine.
N.A.S.A. TND. 5427 (1969).

Printed in England for Her Majesty's Stationery Office by J. W. Arrowsmith Ltd., Bristol 3
Dd 505374 K5 2/75

HER MAJESTY'S STATIONERY OFFICE

Government Bookshops

49 High Holborn, London WC1V 6HB
13a Castle Street, Edinburgh EH2 3AR
41 The Hayes, Cardiff CF1 1JW
Brazennose Street, Manchester M60 8AS
Southey House, Wine Street, Bristol BS1 2BQ
258 Broad Street, Birmingham B1 2HE
80 Chichester Street, Belfast BT1 4JY

Government publications are also available through booksellers

ISBN 0 11 470911 4